Kinetic freeze-out in central heavy-ion collisions between 7.7 and 2760 GeV per nucleon pair

Ivan Melo[1] **and Boris Tomášik**[2,3,4]

[1] Žilinská Univerzita, Akademická 1, 01026 Žilina, Slovakia
[2] Univerzita Mateja Bela, Tajovského 40, 97401 Banská Bystrica, Slovakia
[3] Czech Technical University in Prague, FNSPE, Břehová 7, 11519 Prague, Czech Republic

E-mail: boris.tomasik@cern.ch

CrossMark

Abstract

We fit the single-particle p_t spectra of identified pions, kaons, and (anti)protons from central collisions of gold or lead nuclei at energies between 7.7 and 2760 GeV per nucleon pair. The blast wave model with included resonance production and with an assumption of partial chemical equilibrium is used and the fits are performed with the help of a Gaussian emulator process. A kinetic freeze-out temperature is found about 100 MeV for the lowest collision energies and 80 MeV at the LHC. The average transverse expansion velocity grows with increasing $\sqrt{s_{NN}}$ from 0.45 to 0.65. Due to partial chemical equilibrium, the influence of resonance decays on the shape of the p_t spectra for $\sqrt{s_{NN}}$ above 27 GeV is small.

Keywords: heavy-ion collisions, kinetic freeze-out, blast-wave model

(Some figures may appear in colour only in the online journal)

1. Introduction

The phase diagram of strongly interacting matter can be explored with the help of heavy-ion collisions at various collision energies. The higher the collision energy, the closer the created hot matter to baryon-antibaryon symmetry. It is the purpose of the RHIC Beam Energy Scan (BES) programme to study the dependences of various observables on the collision energy. The ultimate goal of the programme is to explore the QCD phase diagram and possibly find the critical point of the deconfinement phase transition.

---

[4] Author to whom any correspondence should be addressed.

The bulk evolution of the fireball is reflected in the distributions of hadrons that are emitted at the point of their kinetic freeze-out. This is the last moment of the lifetime of the fireball, after it has expanded and cooled down so that no hadrons scatter anymore. By combining information from the single-particle spectra of different hadron species it is possible to reconstruct the freeze-out state of the fireball. This mainly means revealing its temperature and the transverse expansion velocity. This state is the result of the previous expansion due to initial conditions and internal pressure and that, in turn, is conditioned by the properties of the matter: its equation of state and the transport coefficients. Thus—in principle—the knowledge of the final state allows us to deduce the previous evolution and the properties of the matter.

It is then interesting to study the freeze-out state for different collision energies and observe how it changes when the energy is varied.

In this paper we fit the single-particle spectra of pions, kaons, and (anti)protons from central Au+Au or Pb+Pb collisions in the energy range $\sqrt{s_{NN}} = 7.7$ to 2760 GeV. We use the blast-wave model. Also included is the production of resonances from the blast-wave model, which then decay and contribute to the numbers of stable hadrons. The novelty of our approach is in the consistent treatment of the fireball at a lower temperature. Fits to the abundances of the identified hadrons indicate chemical freeze-out temperatures above 145 MeV [1–3]. As we will see, our results for the *kinetic* freeze-out temperature are at least by 40 MeV lower. Despite the lower temperature, the abundances must be observed. This implies chemical potentials that are individual for every hadron species. In a Fermi–Dirac or Bose–Einstein distribution, the presence of chemical potential may change the momentum distribution. Therefore, they are consistently calculated and used here. In practice, as we will show in the paper, at the lower temperature the dominant production moves away from the decays of resonances to a larger portion of hadrons being produced thermally.

The inclusion of resonances is computationally very involved[5]. Therefore, we use DRAGON [5, 6]—a Monte Carlo generator of the final state hadrons—in order to find the best theoretical model. The Bayesian fits then use a Gaussian process emulator for the Markov Chain MC procedure of looking for the best model parameters [7].

There are other similar analyses published in the literature. First of all, the spectra are usually fitted by the experimental collaborations that measure them. ALICE has measured and fitted their p_t spectra from Pb+Pb collisions at $\sqrt{s_{NN}} = 2.76$ GeV in their original publication [8]. In these fits, however, only directly produced hadrons are taken into account and no resonance decays. The same is true for Au+Au collisions at all lower energies studied here, which were measured and fitted by the STAR collaboration [1, 2]. We have fitted the spectra from ALICE in [9] with the model used here, but without the assumption of partial chemical equilibrium. These spectra have also been fitted in [10, 11] with the help of the Cracow single freeze-out model [12, 13] with chemical non-equilibrium. The single freeze-out model has been augmented with sample averaging over events with varying temperature in [14, 15] and fitted to the same data. The blast wave model has been fitted to single-particle distributions from nuclear collisions in a wide interval of collision energies in [16]. There are slight differences to our present treatment, however: that the source is the cut-off in space-time rapidity, and the composition of resonance contributions is taken according to chemical equilibrium. In [17] the spectra are fitted with a two-component blast-wave model, which, however, misses the resonance contribution completely.

Just a few days before finishing this manuscript a similar paper appeared, in which the spectra from ALICE are fitted with the blast-wave model [18]. Resonance decays are included there with the help of a new treatment introduced in [4].

---

[5] Note, however, that in [4] a new computational approach was developed, which makes the calculation of the spectrum with included resonance production more effective.

Our results show that the fireball freezes out at lower temperature and stronger transverse expansion if the collision energy is increased. In addition to that, we also show that for higher collision energies, thanks to the low temperature and the partial chemical equilibrium, the spectra with full resonance production are very similar to those calculated for only directly produced particles.

This paper is structured as follows. In the next section we explain the model. Section 3 deals with the introduction of data which is analysed. In section 4 we present our main results on the temperature and transverse flow and in section 5 we discuss in detail the individual contributions to the spectra from the decays of different resonances. Some semi-quantitative estimates of the p_t dependence of these contributions are deferred to the appendix. We conclude in section 6.

2. The model

The theoretical model used in our analysis is based on the well-known blast wave model [19–23]. The model is formulated with the help of its emission function, which is the Wigner function. For hadrons of the type i, it reads

$$S(x, p)d^4x = g_i \frac{m_t \cosh(\eta - y)}{(2\pi)^3} \left(\exp\left(\frac{p_\mu u^\mu - \mu_i}{T_{\text{kin}}} \right) + s_i \right)^{-1} \theta\left(1 - \frac{r}{R} \right)$$
$$\times \, r \, dr \, d\varphi \, \delta(\tau - \tau_0)\tau \, d\tau \, d\eta. \tag{1}$$

Usually, longitudinal flow dominates the fireball expansion in ultrarelativistic heavy-ion collisions. Therefore, one uses longitudinal proper time $\tau = \sqrt{t^2 - z^2}$ and space-time rapidity $\eta = \frac{1}{2}\ln((t + z)/(t - z))$. In the transverse plane, polar coordinates r, φ are used. Furthermore, T_{kin} is the kinetic freeze-out temperature, m_t the transverse mass and μ_i the chemical potential. We use the proper quantum statistical distributions with $s_i = 1 \, (-1)$ for fermions (bosons) and g_i is the spin degeneracy. Every isospin state is treated separately. The freeze-out time does not depend on radial coordinate, but it does depend on the longitudinal coordinate implicitly via $\tau = \tau_0$, i.e. $t = \sqrt{\tau_0^2 + z^2}$. The density is distributed uniformly within the radius R.

The expansion of the fireball is represented by the velocity field

$$u^\mu = (\cosh\eta_t \cosh\eta, \, \sinh\eta_t \cos\varphi, \, \sinh\eta_t \sin\varphi, \, \cosh\eta_t \sinh\eta) \tag{2}$$

where the transverse velocity is such that

$$v_t = \tanh\eta_t = \eta_f \left(\frac{r}{R} \right)^n. \tag{3}$$

In this relation η_f parametrises the transverse flow gradient and n the profile of the transverse velocity. The mean transverse velocity is then

$$\langle v_t \rangle = \frac{2}{n + 2}\eta_f. \tag{4}$$

This parametrisation of the transverse velocity is taken to be the same as in [1, 2, 4, 8].

The transverse size R and the freeze-out proper time τ_0 influence the total normalisations of the transverse momentum spectra. These parameters also influence the sizes of the HBT radii. A fit that obtains R and τ_0 should thus also take into account the data on HBT radii. Due to computational complexity of such a problem, we choose not to embark on this way and remain without the sensitivity to these geometrical parameters.

From the emission function, one obtains the single-particle spectrum of directly produced hadrons as

$$E\frac{d^3N}{dp^3} = \int_{\Sigma} S(x, p)d^4x,\tag{5}$$

where the integration runs over the whole freeze-out hypersurface. If one replaces the quantum-statistical distribution in equation (1) by the classical Boltzmann distribution and performs some of the integrations in equation (5), one arrives at

$$E\frac{d^3N}{dp^3} = \frac{m_t\tau_0}{2\pi^2}e^{\mu_i/T_{\rm kin}} \int_0^R r\, I_0\left(\frac{p_t}{T_{\rm kin}}\sinh\eta_t(r)\right) K_{\rm l}\left(\frac{m_t}{T_{\rm kin}}\cosh\eta_t(r)\right)dr.\tag{6}$$

This formula is rather easy to evaluate and thus it is often used in the spectra fitting.

Resonances are emitted as described by the emission function in equation (1) and then decay exponentially in time with the mean lifetime given by the inverse of the resonance width. All matrix elements for the decays are assumed to be constant and thus the decay is determined by the phase-space only. We include baryon resonances up to the mass of 2 GeV and mesonic resonances up to 1.5 GeV. An analytical expression for the calculation of the spectra from resonance decays has been derived [20], but it is too cumbersome for frequent evaluation within a fitting routine[6]. Therefore, we use DRAGON for theoretical simulation of the single-particle spectra [5, 6]. This is a Monte Carlo event generator, which produces hadrons (including resonances) according to the emission function (1).

For the contribution from the resonance decays it is also necessary to specify the abundances of every individual resonance species. The final state composition is measured and it is usually found to be in good agreement with the Statistical Hadronisation Model (SHM), which assumes chemical equilibrium with chemical freeze-out temperature $T_{\rm ch}$. However, our results will indicate that the fireball freezes out kinetically at $T_{\rm kin}$ much lower than $T_{\rm ch}$. After the chemical freeze-out, inelastic collisions become rare[7] and the system slips out of the full chemical equilibrium. Nevertheless, in order to keep the abundances of final state stable species fixed, each species develops a non-zero temperature-dependent chemical potential μ_i. At this phase interactions still maintain the *partial chemical equilibrium* between the lowest state stable hadrons and the resonances through which they interact [24]. Also, elastic collisions keep the local thermal equilibrium until the fireball freezes out completely.

Indeed, not all inelastic collisions drop out below $T_{\rm ch}$. For example, $\rho \leftrightarrow \pi\pi$ process remains fast enough to regenerate ρ resonances and, as a consequence, neither the pion number N_π, nor the ρ number N_ρ is fixed, but rather their combination $N_\pi + 2N_\rho$. For the chemical potential this implies $\mu_\rho = 2\mu_\pi$. The number N_ρ continually drops with the temperature decrease while N_π increases until they are finally fixed at $T_{\rm kin}$. Another example may be the Δ^{++} resonance that appears in the process $\pi^+p \leftrightarrow \Delta^{++}$. Hence, $\mu_{\Delta^{++}} = \mu_\pi + \mu_p$. In our calculation, 254 resonance species are included in this way. They are in partial equilibrium with their decay products. Their chemical potentials μ_R are given by the sum of those of the stable decay products μ_i multiplied by the effective numbers of stable hadrons i produced on average from a decay of a resonance R [24]

$$\mu_R = \sum_i N_{i,R}\,\mu_i.\tag{7}$$

---

[6] Note, however, that after we finished our fits, a new treatment has been proposed [4], which should allow for the evaluation of spectra including resonance decays without the need of Monte Carlo simulations.

[7] The relevant (inverse) time scale is the expansion rate $(\partial^\mu u_\mu)$, so 'rare' means a reaction rate much lower than this.
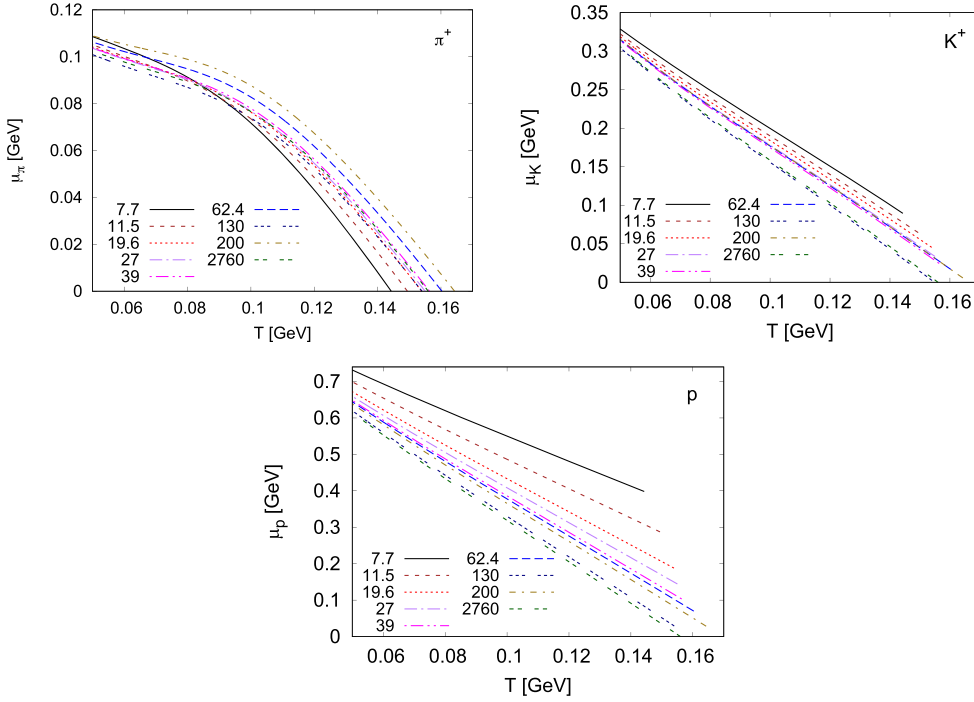
Figure 1. Temperature dependence of the chemical potentials for π^+, K^+, and protons.

Resonances are then let to decay so that in the end we look only at the stable hadrons. In our calculation, the stable species with their own chemical potentials are: π^+, π^-, π^0, K^+, K^-, K^0, $\bar{K}^0$, p, n, $\bar{p}$, $\bar{n}$, Λ, $\bar{\Lambda}$, Σ^+, Σ^-, $\bar{\Sigma}^+$, $\bar{\Sigma}^-$, Ξ^0, Ξ^-, $\bar{\Xi}^0$, $\bar{\Xi}^-$, Ω, $\bar{\Omega}$.

As an example, temperature dependences of the chemical potentials for positive pions, kaons, and protons are shown in figure 1 for different collision energies from the RHIC BES program and the LHC. They were evolved from the temperatures of chemical freeze-out towards lower temperatures. As argued in [24], the evolutions are formulated by requiring that the ratios n_i/s stay independent of temperature. Here, s is the entropy density and n_i the total effective density of stable hadron species i, i.e. the density that includes hadrons which will be produced when all resonances decay. The evolutions always start at the highest temperature in the state of chemical equilibrium. Thus, e.g., protons start with $\mu_p = \mu_B$ at $T_{\rm ch}$, positive kaons start with $\mu_K = \mu_S$, and pions start with $\mu_\pi = 0$ (since we neglect the isospin chemical potential). The initial values for $T_{\rm ch}$, μ_B, and μ_S for each collision energy have been taken from [1–3]. They are summarised in table 1. These values were found to reproduce the *ratios* of hadron multiplicities and we keep them in order to satisfy that observation. Note that shifting these values slightly does not cause a big change in the *shape* of the transverse momentum spectra.

The different sets of $(T_{\rm ch}, \mu_B, \mu_S)$ at the chemical freeze-out lead to different T-dependence of the chemical potentials at different collision energies. As the energy is lowered, $T_{\rm ch}$ decreases. On the other hand, μ_B increases, since the ratio of baryons to antibaryons increases. The pion chemical potential always vanishes in chemical equilibrium at $T_{\rm ch}$. As a result of this behaviour, the ordering of curves for μ_π and μ_p is reversed: at the same temperature, μ_π for $\sqrt{s_{NN}} = 7.7$ GeV is the smallest, because it is evolved from the lowest $T_{\rm ch}$

Table 1. Values of temperature and chemical potentials at the chemical freeze-out from which we start the evolution of the chemical potentials.

$\sqrt{s_{NN}}$ [GeV]	T_{ch} [MeV]	μ_B [MeV]	μ_S [MeV]
7.7	144.3	389.2	89.5
11.5	149.4	287.3	64.4
19.6	153.9	187.9	45.3
27	155.0	144.4	33.5
39	156.4	103.2	24.5
62.4	160.3	69.8	16.7
130	154.0	29.0	2.4
200	164.3	28.4	5.6
2760	156.0	0.0	0.0

of all, with the starting value $\mu_\pi(T_{\mathrm{ch}}) = 0$. In contrast to that, μ_p for $\sqrt{s_{NN}} = 7.7$ GeV is the highest, because it is evolved from the highest μ_B at the chemical freeze-out. The ordering of μ_K follows that of μ_p, because its starting value $\mu_S(T_{\mathrm{ch}})$ follows that of μ_B[8].

The calculated chemical potentials as functions of temperature were tabulated and read in to DRAGON, which used them in the simulations.

3. Data and method

We fitted the transverse momentum spectra of (anti)protons, pions and kaons from the most central heavy-ion collisions measured by STAR and ALICE collaborations:

- Au + Au at $\sqrt{s_{NN}} = 7.7$, 11.5, 19.6, 27, and 39 GeV [1],
- Au + Au at $\sqrt{s_{NN}} = 62.4$, 130, 200 GeV [2],
- Pb + Pb at $\sqrt{s_{NN}} = 2760$ GeV [8].

For $\sqrt{s_{NN}} = 130$ GeV the most central collisions are defined as 0%–6%, for all other remaining energies as 0%–5% of the total cross section.

The fitted intervals vary with energy and particle species. The upper value of p_t was set to 2 GeV for $\sqrt{s_{NN}}$ in the range 7.7–39 GeV (for these energies this was also the upper end of the measured p_t range) and for ALICE spectra, in order to remain in the region sensitive to collective effects and free of hard scattering processes. For $\sqrt{s_{NN}}$ in the range 62.4–200 GeV, the published p_t spectra reach only to about 0.7–1.1 GeV, depending on the species.

The lower end of the fitted intervals coincides with the lower end of the measured p_t range, ranging from $p_t = 0.1$ GeV to $p_t = 0.4$ GeV depending on the collision energy and the species. The only exception (to be discussed in the next section) are the ALICE pion p_t spectra—the data starts at $p_t = 100$ MeV while the fit starts at $p_t = 250$ MeV.

Error bars on the data included statistical and systematic uncertainties as reported in the original papers [1, 2, 8]. We added the two kinds of uncertainties in quadrature.

For data fitting we have used the MADAI statistical analysis package [25]. Theoretical spectra were generated with the DRAGON package described in the previous section. The number of generated events was set to a value that guaranteed that the Monte Carlo statistical

---

[8] A non-vanishing μ_B leads to an imbalance between strange baryons and antibaryons, most notably Λ and $\bar{\Lambda}$. This spoils strangeness neutrality. In order to regain it, a non-zero μ_S is introduced, which then prefers K^+ over K^- and restores strangeness neutrality.
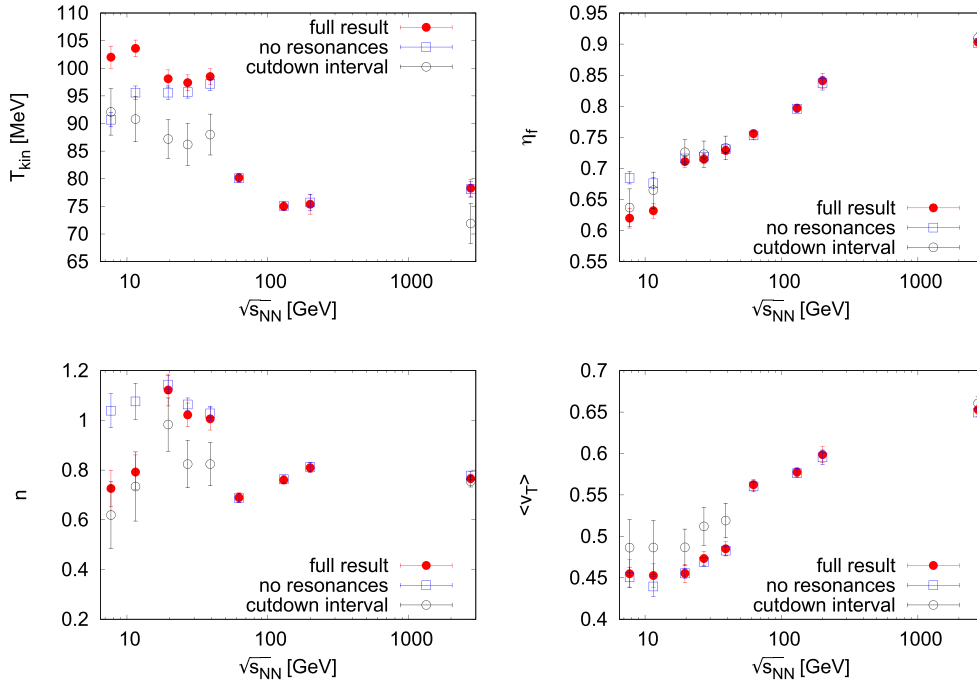
Figure 2. Energy dependence of the freeze-out parameters: temperature (upper left), transverse flow gradient (upper right), exponent of the transverse velocity profile (lower left), mean transverse velocity (lower right).

error was smaller than one third of the combined experimental error in the given p_t bin for every bin and every particle species. This number was thus actually set by antiprotons. The DRAGON spectra were generated typically in 400 training points in the three-parameter space (freeze-out temperature $T_{\rm kin}$, transverse flow gradient η_f, profile of the transverse velocity n). The typical run-time for one training point is 30 min to 5 h depending on the number of events. Then the spectra were normalised to match the normalisation of the measured spectra, species by species, i.e. six independent normalisations.

The essence of MADAI is the Markov Chain Monte Carlo exploration of the parameter space weighted by the posterior probability, or likelihood for a particular point $T_{\rm kin}$, η_f, n to represent the correct parameters given the experimental observations. The likelihood for points other than training points is not calculated from DRAGON (which is time consuming) but rather estimated from the Gaussian-process-based emulator trained on the training points. The output of MADAI is the best fit point in our three-parameter space. The uncertainties and correlations among parameters can be displayed as two-dimensional projections of the posterior distribution. As a final step (and a cross-check of MADAI), we calculated the χ^2 value at the best fit point.

4. Results

The main results of this paper, the energy dependences of the kinetic freeze-out temperature $T_{\rm kin}$, the transverse flow gradient η_f, the profile of the transverse velocity n, and the mean transverse velocity $v_t = 2\eta_f/(n + 2)$, are shown in figure 2. Three sets of results are plotted:

Table 2. Parameters of the best fits for different energies. These parameters were used also for the calculation of the resonance composition of the transverse momentum spectra.

$\sqrt{s_{NN}}$ [GeV]	T_{kin} [MeV]	η_f	n	χ^2/n_{dof}
7.7	102.0 ± 2.0	0.620 ± 0.016	0.726 ± 0.073	0.83
11.6	103.6 ± 1.5	0.632 ± 0.012	0.792 ± 0.069	0.66
19	98.1 ± 1.6	0.711 ± 0.009	1.122 ± 0.064	0.38
27	97.4 ± 1.4	0.715 ± 0.007	1.022 ± 0.048	0.68
39	98.5 ± 1.4	0.729 ± 0.007	1.006 ± 0.045	0.47
62	80.2 ± 0.8	0.756 ± 0.007	0.689 ± 0.020	0.93
130	75.0 ± 0.8	0.797 ± 0.006	0.760 ± 0.015	1.07
200	75.4 ± 1.8	0.841 ± 0.012	0.810 ± 0.020	0.25
2760	78.3 ± 1.6	0.903 ± 0.005	0.766 ± 0.018	0.32

the full results obtained from fits to p_t spectra up to 2 GeV, which include the contribution from the resonance decays (solid red circles), results from fits to p_t spectra up to 2 GeV without the resonance contribution (blue squares) and finally results from fits to short (cut down) p_t spectra up to ~1 GeV, which match shorter p_t intervals for $\sqrt{s_{NN}} = 62, 130, 200$ GeV with the resonance contribution included (empty black circles). For the full results we summarise the corresponding numerical values of T_{kin}, η_f and n together with the χ^2/n_{dof} value in table 2.

The freeze-out temperature decreases from $T_{\text{kin}} \sim 100$–104 MeV at the lowest energies to $T_{\text{kin}} \sim 75$–80 MeV at the highest energies. There is a little jump between $\sqrt{s_{NN}} = 39$ and 62.4 GeV (full results, solid red circles). This is most likely caused by the difference in p_t intervals, which are covered by the data. Recall that we usually fit spectra up to $p_t = 2$ GeV, while the upper limit of the published spectra at 64.2–200 GeV is around 0.8 GeV for mesons and 1.1 GeV for protons. Indeed, once the p_t intervals are matched (empty black circles), the jump is suppressed, although a steady decrease of T_{kin} with increasing $\sqrt{s_{NN}}$ remains. The effect of resonances is negligible at high energies while at the lowest energies they induce an upward shift in the temperature of the order of 10 MeV. As we will see in the next section, this is caused by the lower population of particles from resonance decays and also by the uniform relative contribution to p_t spectra at high energies.

The transverse flow gradient increases from $\eta_f = 0.62$ at $\sqrt{s_{NN}} = 7.7$ GeV to $\eta_f = 0.90$ at $\sqrt{s_{NN}} = 2760$ GeV. The effect of resonances is again significant only at the two lowest energies. The profile of the transverse velocity n is the least sensitive parameter but one might conclude that it is roughly consistent with a constant value $n \sim 0.75$ once the lower energies are cut down to the short p_t range. The mean transverse velocity increases with energy from $v_t = 0.45$ to $v_t = 0.65$.

In figure 3 two-dimensional projections of the posterior distribution are plotted for (a) $\sqrt{s_{NN}} = 7.7$ GeV and (b) $\sqrt{s_{NN}} = 2760$ GeV. We can see the uncertainty region around the best fit parameters and also the correlation/anticorrelation among the parameters. For example, the temperature and the transverse flow gradient are anticorrelated in the sense that a slight decrease of T_{kin} can be compensated by an increase of η_f with little effect on the quality of the fit. Also illustrated is a larger uncertainty of the best fit for $\sqrt{s_{NN}} = 7.7$ GeV, driven by the experimental errors (this is true also for $\sqrt{s_{NN}}$ in the range 11.5–39 GeV).

The simulated transverse momentum spectra of p, π^+ and K^+, corresponding to the best fit parameters (full results in figure 2 and table 2) are displayed in figures 4–6 for different

(a) $\sqrt{s_{NN}} = 7.7$ GeV

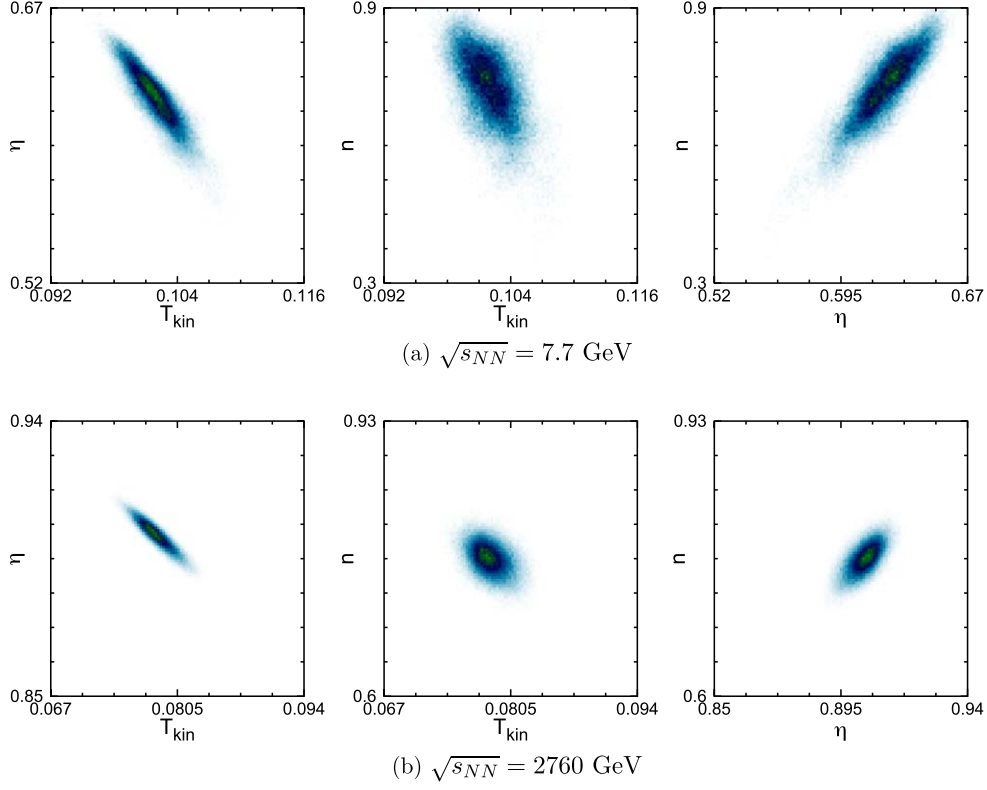

(b) $\sqrt{s_{NN}} = 2760$ GeV

Figure 3. Two-dimensional projections of the posterior distribution for a) $\sqrt{s_{NN}} = 7.7$ GeV, b) $\sqrt{s_{NN}} = 2760$ GeV: $\eta_f - T_{\text{kin}}$ (left column), $n - T_{\text{kin}}$ (middle column), $n - \eta_f$ (right column).

energies as solid lines along with the measured data points (including uncertainties) from STAR and ALICE. The ratio of data to Monte Carlo simulation, $N_i^{\text{exp}}/N_i^{MC}$, is shown with errors in figures 7–9.

The general quality of the fits for all energies, particle species and the whole p_t range is violated by the low p_t pions at $\sqrt{s_{NN}} = 2760$ GeV where Monte Carlo underestimates the data (the first six p_t bins were excluded from the fit in this case). Similar disagreement has also been observed in [17]. There are at least two effects, both included in our simulation, which help populate this p_t region: pions originating from the resonance decays and the non-zero pion chemical potential ~ 100 MeV. We note that this disagreement with the data can be explained within the context of chemical non-equilibrium version of the statistical hadronization model [10]. Note, however, that the enhancement of the pion spectrum at low p_t with respect to the theoretical curve may well be caused by a specific shape of the freeze-out hypersurface in which the matter at larger distance from the longitudinal axis of the fireball freezes-out later than the matter in the middle[9]. Such a hypersurface was used in the fits reported in [14], which show better agreement with pions at low p_t.

---

[9] Technically, this is caused by a decreased flux of particles with higher p_t through such a freeze-out hypersurface. Hence, it is the high p_t that becomes suppressed, thus leaving the non-suppressed low p_t to look like it was enhanced.
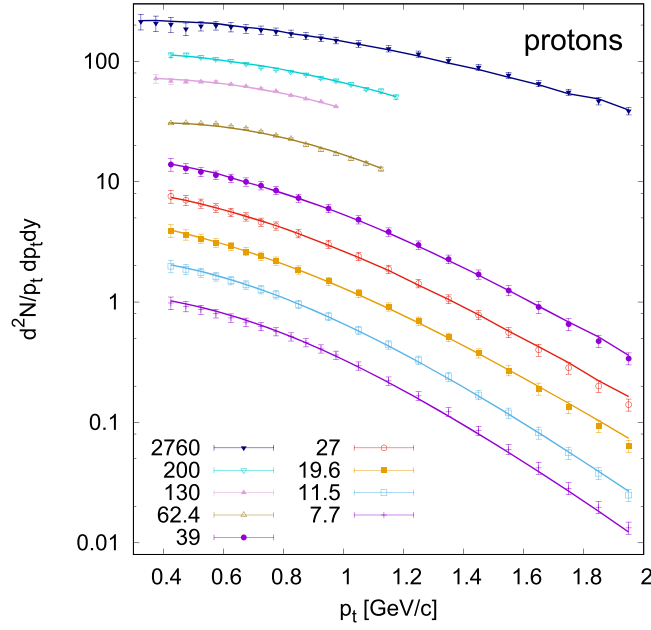
Figure 4. Transverse momentum spectra of protons for different energies. In order to display all spectra in one figure we divide data for $\sqrt{s_{NN}} = 7.7, 11.5, 19.6, 27, 39, 62.4, 130, 200, 2760$ GeV by factors 256, 128, 64, 32, 16, 8, 4, 2 and 0.5, respectively.

5. Anatomy of the spectra

Let us come back to the observation, that the effect of resonance decays on the extracted T_{kin} is negligible at high $\sqrt{s_{NN}}$, while they cause a slight upward shift at low $\sqrt{s_{NN}}$. In order to understand this we have looked at the composition of the p_t spectra—how does the origin of all observed pions (kaons, protons) depend on p_t? Results for five chosen energies, $\sqrt{s_{NN}} = 7.7, 11.5, 27, 200, 2760$ GeV, are plotted in figures 10–12. The values of the parameters used in the calculations of these figures are summarised in table 2.

We observe some systematics connected with the change of the collision energy:

 (i) The fraction of resonance-produced hadrons decreases as the collision energy goes up. This may seem surprising at the first sight. However, this behaviour is closely connected with the scenario of partial chemical equilibrium. The share of resonance production is high at the moment of the chemical freeze-out. Afterwards, however, the temperature decreases and even though chemical potentials develop for all resonance species, the weight of particle production moves from resonances towards directly produced particles.

(ii) At lower collision energies the resonances populate the low p_t interval more while at 200 GeV and higher the share of resonance production seems to be rather flat as function of p_t. This change is actually gradual. A closer inspection reveals that the feature is mainly brought in by the Δ resonance. Its decay happens closely above the threshold, so that daughter particles do not acquire high momentum. In combination with small transverse expansion velocity, this causes pions from such decays to stay at low p_t. (A similar argument applies for kaons from the decay of ϕ.) Let us also stress that at lower
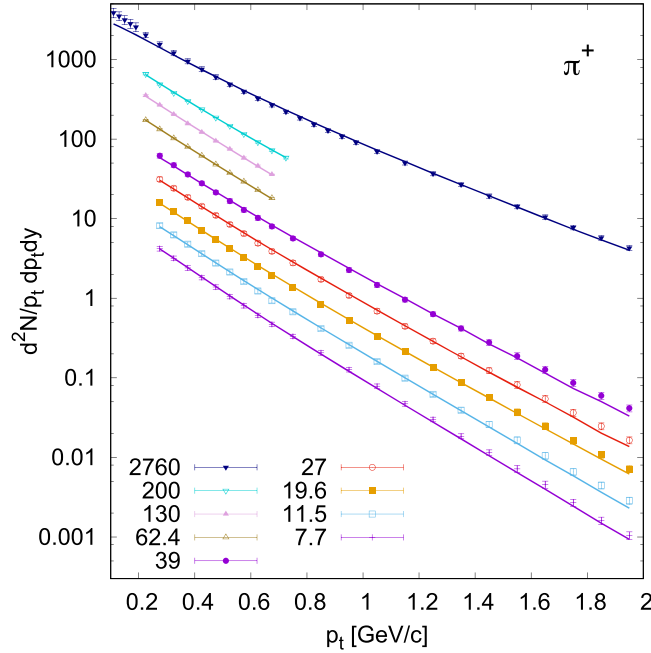
Figure 5. Transverse momentum spectra of π^+ for different energies. In order to display all spectra in one figure we divide data for $\sqrt{s_{NN}} = 7.7$, 11.5, 19.6, 27, 39, 62.4, 130, 200, 2760 GeV by factors 256, 128, 64, 32, 16, 8, 4, 2 and 0.5, respectively.

energies the contribution from *baryon* resonances (most importantly Δ) to pion production is more important than at higher energies. A semi-quantitative discussion of this feature is presented in the appendix.

We have also explored how these results change if T_{kin} is varied within the confidence regions as indicated in figure 3. The changes in the composition of the p_t spectrum can be barely seen in the figures, so we refrain from showing them here. If T_{kin} is decreased to the edge of the confidence interval (which is usually a shift smaller than 2 MeV), generally the fractions of directly produced hadrons increase their values by a few per cent. The increase is slightly larger at low p_t than at high p_t, and also it is larger at low $\sqrt{s_{NN}}$ than at high $\sqrt{s_{NN}}$.

6. Conclusions

Our results clearly show that with the increase of the collision energy the fireball develops stronger transverse expansion and cools further down. The former feature is well expected. The decrease of temperature by more than 20 MeV can also be understood: more energy and entropy is deposited in the collision, which expands to a larger volume. At larger volume the local (longitudinal) flow gradients are smaller and so is the expansion rate. Thus, also the scattering rate at the freeze-out drops lower, and so does the temperature. To confirm this scenario we would need to extract the sizes of the fireball with the help of femtoscopy. This goes beyond the scope of the present paper and we leave it for further investigation.

Although the excitation function of the kinetic freeze-out temperature seems to show a sharp step between 39 and 62.4 GeV, it would be premature to make any conclusions out of
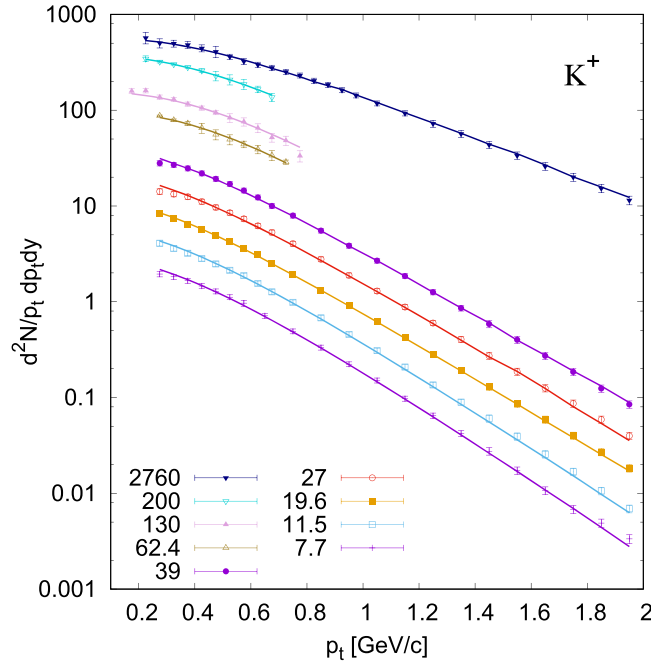
Figure 6. Transverse momentum spectra of K^+ for different energies. In order to display all spectra in one figure we divide data for $\sqrt{s_{NN}} = 7.7, 11.5, 19.6, 27, 39, 62.4, 130, 200, 2760$ GeV by factors 256, 128, 64, 32, 16, 8, 4, 2 and 0.5, respectively.

this. The feature may be connected with the different coverage of p_t intervals in the different data sets.

It is interesting to observe that the results obtained with the full model with resonances coincide with those obtained with only directly produced hadrons, i.e. basically just with fitting the formula (6). This is seen for all but the two lowest collision energies. It is crucial here that the partial chemical equilibrium was assumed, as a consequence of the cooling of the fireball between the chemical and the thermal freeze-out. The cooling is most pronounced at high collision energies where the temperature drops from about 160 MeV to some 80 MeV, i.e. by 80 MeV. In contrast to that, at $\sqrt{s_{NN}} = 7.7$ GeV it went down only by roughly 40 MeV between 144 and 102 MeV. In view of these numbers it is clearly understood that the influence of resonances becomes less important at high energies.

We hoped originally that we would be able to fit the low p_t enhancement of the pion spectra at the LHC, since pions develop chemical potential about 90 MeV at the kinetic freeze-out temperature. Note that a successful fit was obtained with the non-equilibrium Cracow single freeze-out model[10] with a possible admixture of pion condensation [26]. Nevertheless, the enhancement may also be caused by a specific shape of the freeze-out hypersurface used in [26], which corresponds to an inside-out freeze-out in transverse direction [27]. Such features have never been explored in the blast-wave-like fits and this opens the question of whether or not it is worth studying.

---

[10] Note that in the Cracow single freeze-out model, non-equilibrium refers to the feature where chemical equilibrium is not reached even at the chemical freeze-out, unlike in our model here.
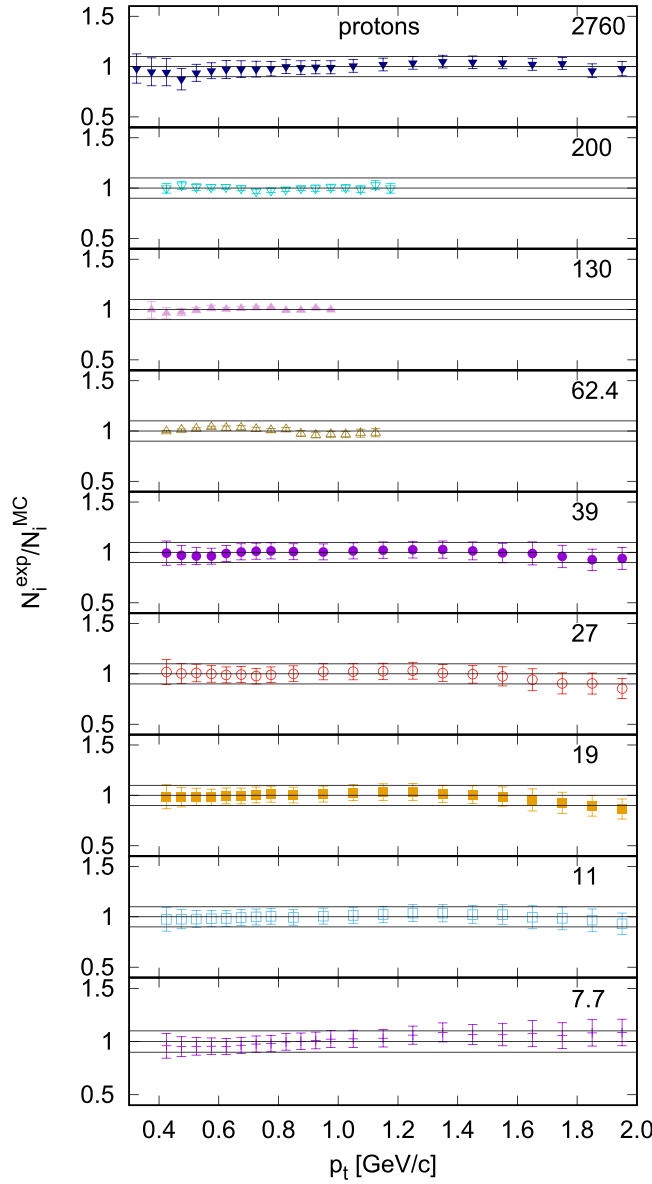
Figure 7. The ratio of data to Monte Carlo simulation, $N_i^{\exp}/N_i^{MC}$ for p_t spectra of protons. Different panels show the ratios for different collision energies. Horizontal lines indicate a band between 0.9 and 1.1.

The least well-determined parameter of the model is the exponent n. It might be consistent with a constant value if the cuts on spectra are applied. Clearly, spectra in broader p_t intervals also at $\sqrt{s_{NN}} = 62.4$, 130, and 200 GeV are necessary in order to settle this uncertainty. Nevertheless, full experimental results seem to indicate that n decreases as the $\sqrt{s_{NN}}$ grows. This may be purely a kinematically determined feature. The transverse velocity profile of equation (3) is constructed so that it never grows above 1. However, in a real fireball the velocity at the edge may get closer to this limit. At this point, relativity kicks in. As the
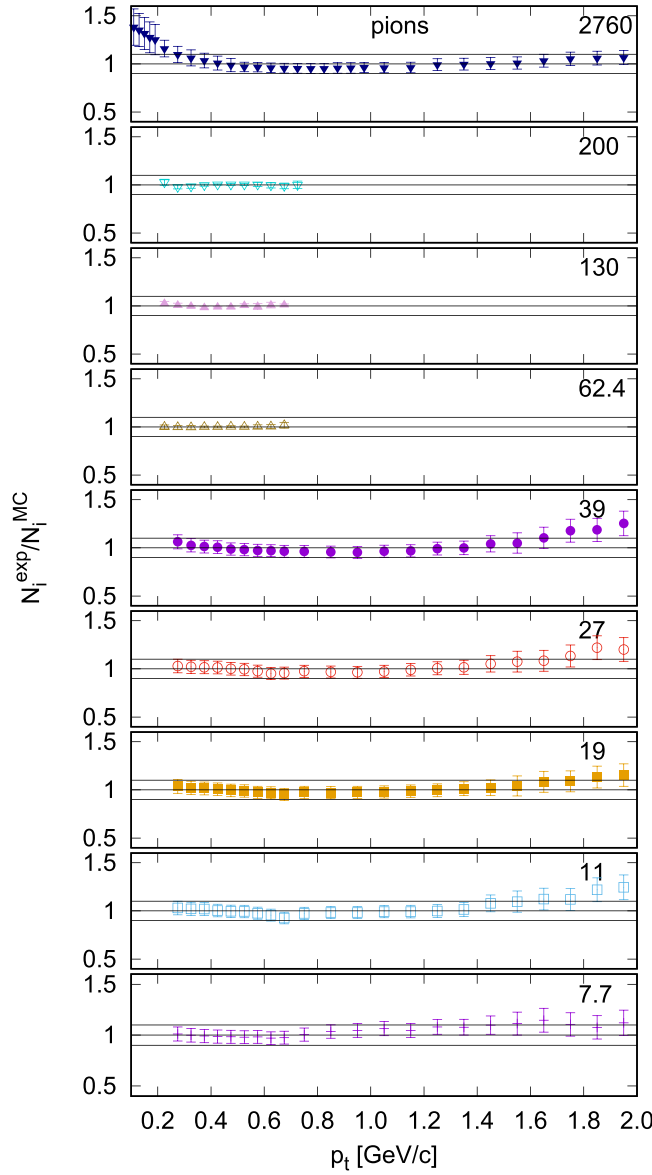
Figure 8. The ratio of data to Monte Carlo simulation, $N_i^{\mathrm{exp}}/N_i^{MC}$ for p_t spectra of π^+. Different panels show the ratios for different collision energies. Horizontal lines indicate a band between 0.9 and 1.1.

matter is locally boosted to a higher transverse velocity, then due to the Lorentz transformation of the velocity into the global frame the dependence $v_t(r)$ begins to level off. The concave dependence in our model is parametrised by n with values smaller than 1.

We do not want to conclude without mentioning the results of [18], which appeared just days before the submission of our paper. Apparently, spectra from the ALICE experiment have been fitted there with the same model as we used here, but the resonance contribution has been determined with the help of a novel method [4] that avoids MC simulations. At
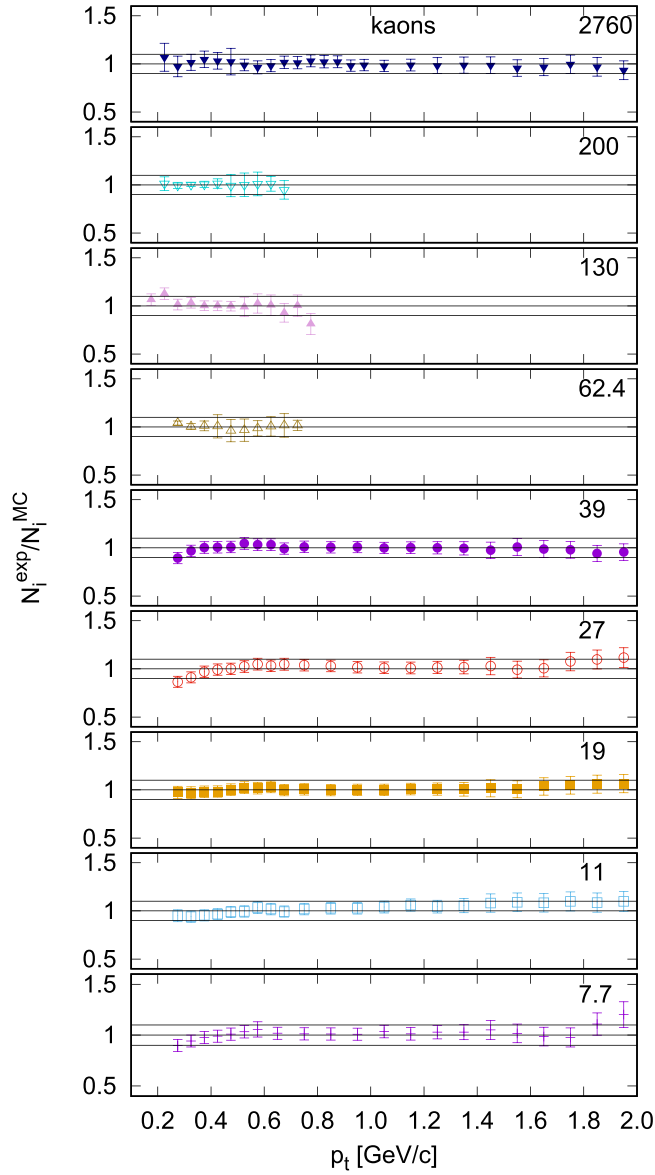
Figure 9. The ratio of data to Monte Carlo simulation, $N_i^{\exp}/N_i^{MC}$ for p_t spectra of K^+. Different panels show the ratios for different collision energies. Horizontal lines indicate a band between 0.9 and 1.1.

$\sqrt{s_{NN}} = 2.76$ TeV their result in the partial chemical equilibrium in central Pb+Pb collisions is $T_{\rm kin} = 127 \pm 2$ MeV. Presently, we do not have an explanation for this difference. To the extent we can judge from [18], the only difference is that the lists of stable species in the partial chemical equilibrium there and in our work are different. It will be important and interesting to sort out this tension in the near future.
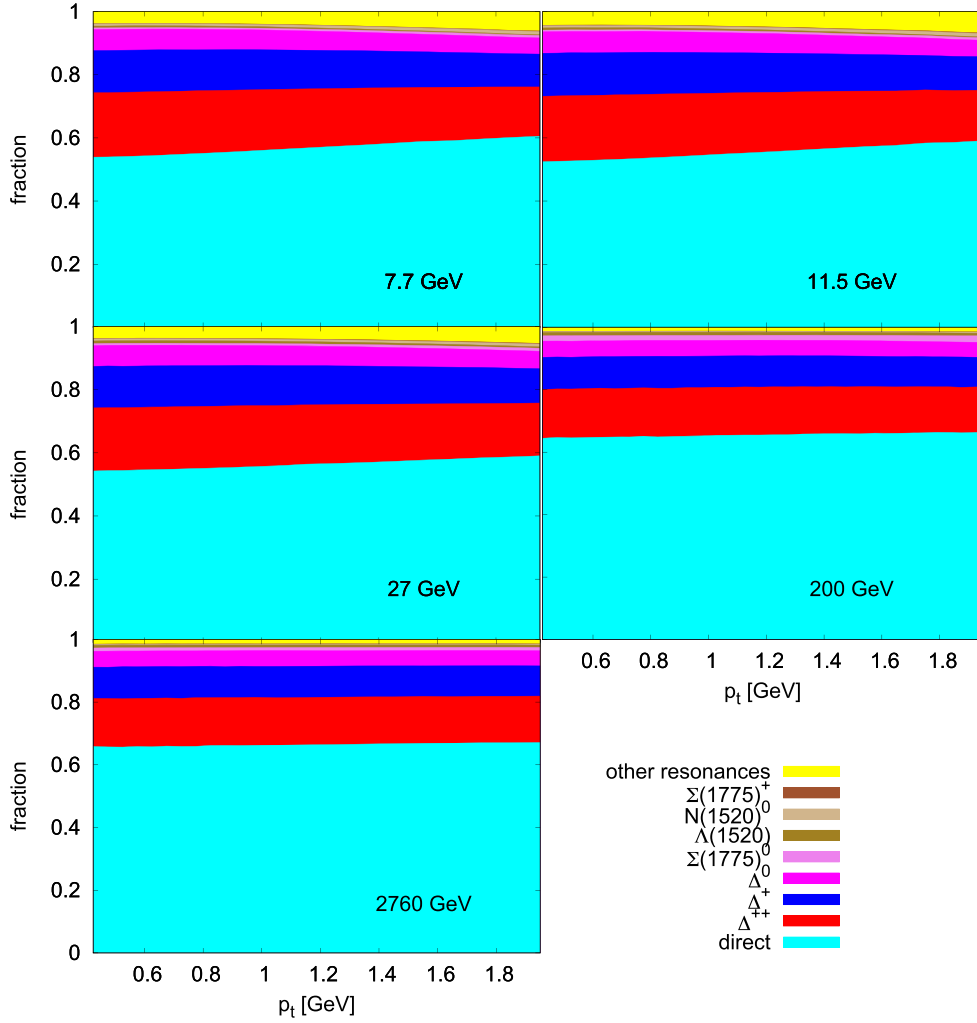
Figure 10. The anatomy of the p_t spectra of protons from collisions at $\sqrt{s_{NN}} = 7.7, 11.5, 27, 200$ and 2760 GeV. The ratios of protons of a given origin (direct or from a particular resonance) to the total number of protons as function of p_t are plotted. The bands from the bottom show the relative contributions from direct protons, protons from Δ^{++}, Δ^+, Δ^0,...

In this paper we presented results of a pilot study where only data from *central* collisions have been fitted. A more comprehensive study, which will also include the centrality dependence, is being elaborated and will be published later.

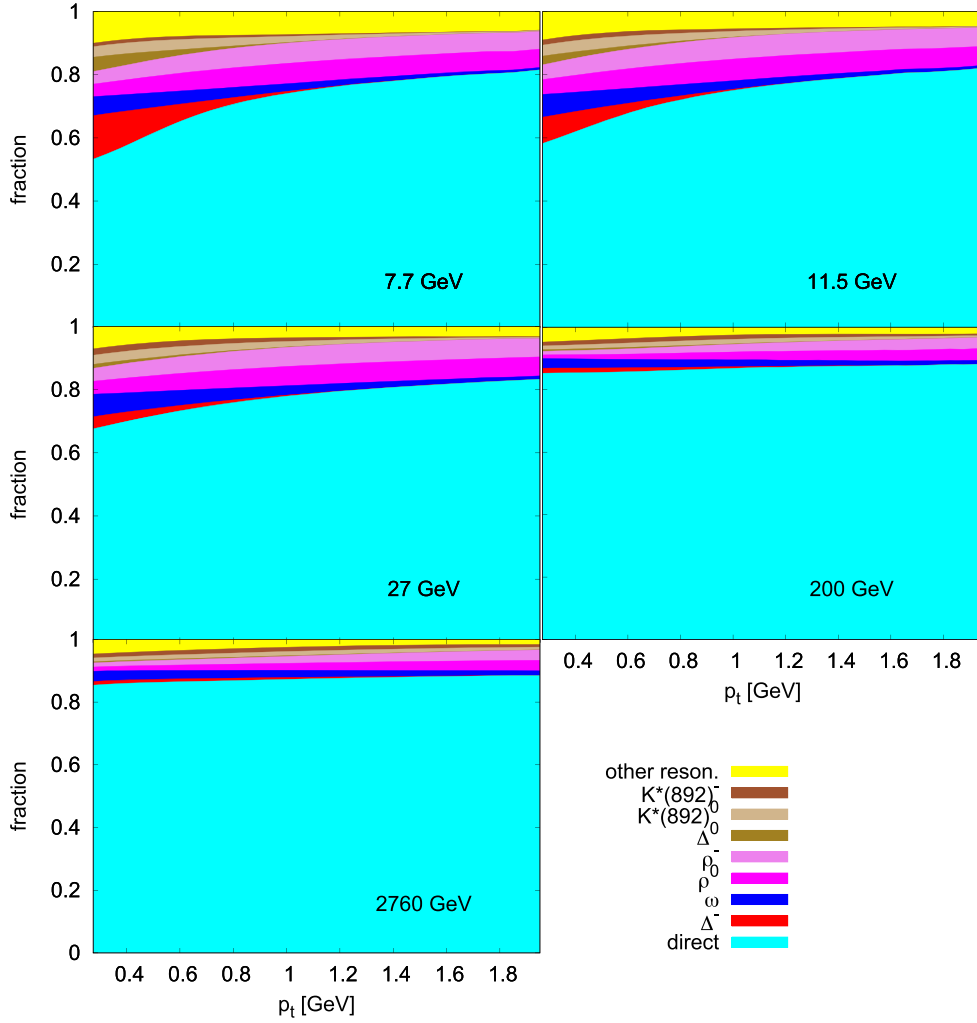## Acknowledgments

Figure 11. The anatomy of the p_t spectra of π^- from collisions at $\sqrt{s_{NN}} = 7.7, 11.5, 27, 200$ and 2760 GeV. The ratios of π^- of a given origin (direct or from a particular resonance) to the total number of π^- as functions of p_t are plotted. The bands from bottom show the relative contributions from direct π^-, pions from Δ^-, ω, ρ^0, ρ^-,...

Appendix. Estimates of hadron momentum from resonance decays

In this appendix, we seek some back-of-the-envelope understanding of why the resonance contribution to the p_t-spectra is different at different energies. This definitely does not replace
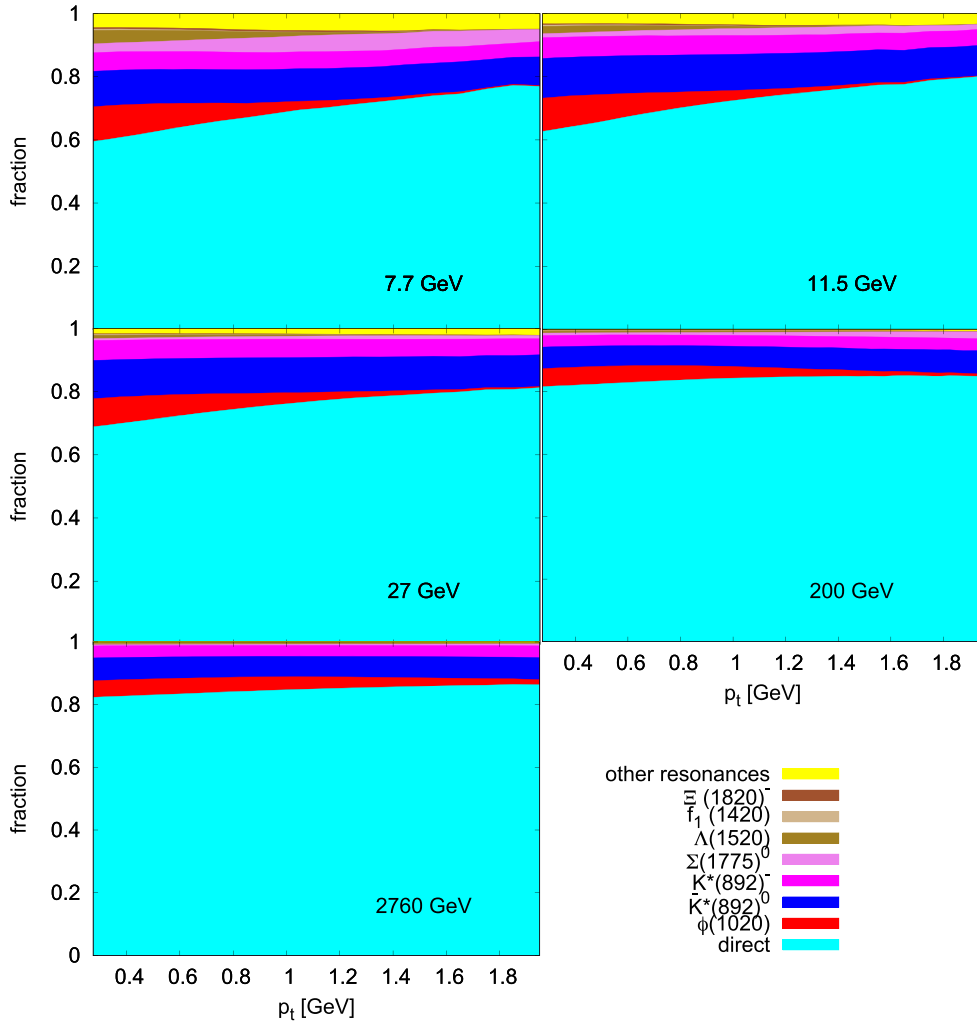
Figure 12. The anatomy of the p_t spectra of K^- from collisions at $\sqrt{s_{NN}} = 7.7, 11.5, 27, 200$ and 2760 GeV. The ratios of K^- of a given origin (direct or from a particular resonance) to the total number of K^- are plotted. The bands from the bottom show the relative contributions from direct K^-, kaons from ϕ, $\bar{K}(892)^0$, $K(892)^-$,...

the full calculation that convolutes the spectra of resonances with the phase space available for the decay, and which was effectively done when we simulated the spectra and calculated the ratios shown in figures 10–12. A closer inspection of those figures shows that contributions to the p_t spectrum, which are not flat in p_t, are due to resonances with masses close above the sum of the masses of the daughter particles. The most notable is the decay $\Delta \rightarrow N\pi$. In such decays, the decay products acquire only small kinetic energy[11]. For example, the total kinetic energy released in the decay of Δ is 155 MeV.

---

[11] The natural scale, to determine what is small and what is big, is provided by the temperature. Energies, which are comparable to T, we call small.

Let us try to understand why the contributions of resonance decays populate pion spectra mainly at low p_t in collisions at $\sqrt{s_{NN}} = 7.7$ GeV, while they are flat in p_t at 200 GeV and higher energies.

At lower collision energies, also the transverse expansion of the fireball is weaker. The heavy resonances follow more closely the collective velocity of the fluid and do not depart from it with thermal velocities too much. Thus there is only small boost in the transverse direction and pions (nucleons) are produced with small momenta from the decays of such resonances. However, at higher collision energies, the transverse expansion is stronger and the heavy resonances also obtain a stronger boost in that direction, depending on their position in the fireball. Thanks to this boost, the resonance decays can also populate daughter particles with higher p_t.

We illustrate these qualitative considerations with some simple estimates. First, the momentum of the pion from a decay of Δ in the rest frame of the Δ is

$$p = \frac{\sqrt{(M^2 - m_\pi^2 - m_N^2)^2 - 4m_\pi^2 m_N^2}}{2M}, \tag{A.1}$$

where M is the mass of the resonance. For the decay $\Delta \to N\pi$ we obtain $p = 227.7$ MeV. This gives the total energy for the pion 266.8 MeV and its share of the released kinetic energy is 127 MeV (out of the quoted 155 MeV).

Now we want to estimate the maximum p_t that we can expect for a pion emitted from a Δ-resonance, which is boosted transversely due to the expansion of the fireball.

If the Δ resonance moves with velocity v, and the pion is emitted in the direction of the collective velocity, its transverse momentum is boosted to the lab frame

$$p_{lab} = \gamma p + v\gamma E_\pi, \qquad \text{with} \quad \gamma = \frac{1}{\sqrt{1 - v^2}}, \tag{A.2}$$

where E_π is the energy of the pion.

In addition to the flow velocity, the resonance also has some random thermal velocity, which we also want to estimate. Since its total energy is the sum $m + E_{kin}$ and the kinetic energy is given by the temperature, we have

$$\gamma_{th} = \frac{m + E_{kin}}{m} = \frac{m + T}{m} \tag{A.3}$$

which gives

$$v_{th} = \frac{\sqrt{2mT + T^2}}{m + T}. \tag{A.4}$$

Let us now estimate the typical p_t scale, which can be reached by pions from Δ decays. We do this for two values of $\sqrt{s_{NN}}$, the lowest and the highest energy.

7.7 GeV The transverse expansion velocity at the edge of the fireball is 0.62, and the γ factor is then 1.275. Suppose a Δ resonance moving with this velocity. In order to estimate the maximum p_t a pion can obtain from a Δ-decay, suppose the pion from this Δ moves in the same direction. According to equation (A.2) it acquires the p_t of 500 MeV. On top of this the Δ also moves with random thermal velocity about 0.37 in the fluid rest frame. This velocity is directed randomly, so it will boost some pions to higher p_t and some to lower p_t. We conclude that pions from Δ decays will reach up to p_t of about 500 MeV.

2760 GeV We proceed similarly for the fireball at the highest energy. The transverse expansion velocity at the edge of the fireball is 0.903 and the γ factor is then 2.327. If the pion from the decay is boosted with this velocity according to equation (A.2), it acquires the momentum 1 090.5 MeV. Thermal velocity of the Δ is 0.33.

We basically see that there is not a big difference between the thermal boost velocities in the two cases. Hence, we expect that at 7.7 GeV the contribution to pion production from Δ decays will reach up to 500 MeV, while at 2760 GeV it should go to 1090 MeV. These limits are then blurred by the thermal smearing, which is comparable in both cases. This explains the different p_t dependences of the relative contribution to pion p_t spectra at different energies.

ORCID iDs

Boris Tomášik ⓘ https://orcid.org/0000-0003-0478-0609

References

[1] Adamczyk L *et al* (STAR collaboration) 2017 *Phys. Rev.* C **96** 044904
[2] Abelev B I *et al* (STAR collaboration) 2009 *Phys. Rev.* C **79** 034909
[3] Milano L and (ALICE Collaboration) 2013 *Nucl. Phys.* A **904–905** 531c
[4] Mazeliauskas A, Floerchinger S, Grossi E and Teaney D 2019 *Eur. Phys. J.* C **79** 284
[5] Tomášik B 2009 *Comput. Phys. Commun.* **180** 1642
[6] Tomášik B 2016 *Comput. Phys. Commun.* **207** 545
[7] Rasmussen C E and Williams C K I 2006 *Gaussian Processes for Machine Learning* (Cambridge, MA: The MIT Press) http://gaussianprocess.org/
[8] Abelev B *et al* (ALICE collaboration) 2013 *Phys. Rev.* C **88** 044910
[9] Melo I and Tomasik B 2016 *J. Phys.* G **43** 015102
[10] Begun V, Florkowski W and Rybczyński M 2014 *Phys. Rev.* C **90** 014906
[11] Begun V, Florkowski W and Rybczyński M 2014 *Phys. Rev.* C **90** 054912
[12] Broniowski W and Florkowski W 2001 *Phys. Rev. Lett.* **87** 272302
[13] Chatterjee S, Mohanty B and Singh R 2015 *Phys. Rev.* C **92** 024917
[14] Prorok D 2016 *J. Phys.* G **43** 055101
[15] Prorok D 2019 *Eur. Phys. J.* A **55** 37
[16] Rode S P, Bhaduri P P, Jaiswal A and Roy A 2018 *Phys. Rev.* C **98** 024907
[17] Li L L and Liu F H 2018 *Eur. Phys. J.* A **54** 169
[18] Mazeliauskas A and Vislavicius V 2020 *Phys. Rev.* C **101** 014910
[19] Siemens P J and Rasmussen J O 1979 *Phys. Rev. Lett.* **42** 880
[20] Schnedermann E, Sollfrank J and Heinz U 1993 *Phys. Rev.* C **48** 2462
[21] Csörgő T and Lörstad B 1996 *Phys. Rev.* C **54** 1390
[22] Tomášik B, Wiedemann U A and Heinz U 2003 *Heavy Ion Phys.* **17** 105
[23] Retiere F and Lisa M A 2004 *Phys. Rev.* C **70** 044907
[24] Bebie H, Gerber P, Goity J L and Leutwyler H 1992 *Nucl. Phys.* B **378** 95
[25] Novak J, Novak K, Pratt S, Coleman-Smith C E and Wolpert R L 2014 *Phys. Rev.* C **89** 034917
[26] Begun V and Florkowski W 2015 *Phys. Rev.* C **91** 054909
[27] Sochorová R 2016 *Bachelor Thesis* Czech Technical University in Prague